Published in final edited form as:
IEEE Antennas Wirel Propag Lett. 2010 March 18; 9: 268–. doi:10.1109/LAWP.2010.2045871.

Dual-Band Miniaturized Patch Antennas for Microwave Breast Imaging

Mudar A. Al-Joumayly, **Suzette M. Aguilar**, **Nader Behdad**, and **Susan C. Hagness**
Department of Electrical and Computer Engineering, University of Wisconsin-Madison, Madison, WI 53706 USA

Mudar A. Al-Joumayly: aljoumayly@wisc.edu; Suzette M. Aguilar: smaguilar@wisc.edu; Nader Behdad: behdad@engr.wisc.edu; Susan C. Hagness: hagness@engr.wisc.edu

Abstract

We present a miniaturized, dual-band patch antenna array element that is designed for use in a 3-D microwave tomography system for breast imaging. Dual-band operation is achieved by manipulating the fundamental resonant mode of the patch antenna and one of its higher-order modes. Miniaturization and tuning of the resonant frequencies are achieved by loading the antenna with non-radiating slots at strategic locations along the patch. This results in a compact, dual-band antenna with symmetric radiation patterns and similar radiation characteristics at both bands of operation. The performance of the antenna in a biocompatible immersion medium is verified experimentally.

Index Terms

microstrip antennas; multifrequency antennas; microwave imaging; breast cancer detection

I. Introduction

It is crucial for clinicians around the world to have access to affordable, non-ionizing, three-dimensional (3-D) tomographic and quantitative breast imaging tools that will aid them in screening women at higher risk for breast cancer [1] as well as monitoring changes in breast tissue in response to prevention and treatment protocols [2]. Recent investigations suggest that low-cost non-ionizing microwave tomography is well-suited for this type of imaging application (see, for example, [3]–[10]). In microwave tomography, low-power microwave signals are transmitted into the breast tissue by an array of antennas, the scattered signals are measured, and the spatial distribution of the dielectric properties throughout the breast volume are estimated by solving an electromagnetic nonlinear inverse scattering problem. A study presented in [11] shows that the degree of ill-posedness of the inverse problem varies with the number and location of observations, the number of frequencies used, and the spatial resolution provided by the illuminating wavelengths. The antenna elements used in the sensor array have a direct impact on these factors, and thus, on the accuracy of microwave breast imaging.

The 3-D antenna array that surrounds the breast of a prone patient is ideally composed of a large number of elements to permit dense 3-D spatial sampling of scattered fields. Thus each antenna element should occupy a very small footprint relative to the total surface area of the breast. In addition, it is advantageous for the miniaturized antennas to operate efficiently at multiple frequencies. Solving the inverse scattering problem at a single frequency poses inherent challenges because the stability and resolution of the imaging algorithm represent competing demands in choosing the frequency [12]. In contrast, the advantages of both

lower and higher frequencies are retained with a multi-frequency approach [13]. The use of a parametric model to reconstruct the frequency-dependent dielectric properties reduces the ill-posed nature of the inverse problem [14] and computational burden of the multi-frequency algorithm [8]. In particular, antenna elements that operate within the frequency range of 0.5–3.0 GHz are desired. Frequencies below and above this range are non-optimal in terms of spatial resolution and penetration depth, respectively. In addition, the antenna needs to operate in an immersion medium that improves coupling efficiency of the low-power microwave signals into and out of the breast. Finally, the antenna design should not be so complex as to render it impractical to model in the reconstruction algorithm.

This letter reports a multi-frequency miniaturized patch antenna array element designed for use in a 3-D microwave tomography system. Our proposed antenna, which has been specifically designed to meet the specifications described above, offers several advantages over what are arguably the most widely used radiating elements in microwave tomography, namely monopole and dipole antennas [6], [9], [15], [16]. Monopoles and dipoles, as well as simple patches and slots, offer simplicity in terms of forward-problem modeling and may be impedance matched across a wide bandwidth when immersed in a lossy medium. However, this broadening of the bandwidth is done through the addition of loss into the system and at the expense of reducing the radiation efficiency of the antenna over a large bandwidth [17]. Our rationale for using a multi-band antenna stems in part from the expectation that the higher gain exhibited at the design frequencies will provide a higher signal-to-noise ratio and imaging sensitivity when immersed in a low-loss coupling medium. The planar design of our proposed antenna elements also offers several added benefits. The ground plane backing prevents undesired illumination of scatterers outside of the breast and thereby avoids environmental interference that can occur with omnidirectional radiators. Furthermore, the antenna characteristics are independent of the coaxial feed cables. This isolation increases the accuracy of the antenna modeling required in the forward simulations of the inverse scattering algorithm, which we conduct using the finite-difference time-domain (FDTD) method (e.g. [10]). The planar design and relatively large feature sizes of the proposed antenna contribute to its ease of modeling using FDTD.

II. Antenna Design

The antenna is designed to operate in a biocompatible immersion medium comprised of safflower oil. We characterized the dielectric properties of the immersion medium over the frequency range of interest (0.5 GHz – 3 GHz) using an Agilent 85070D dielectric probe kit and E8364 vector network analyzer (VNA). A single-pole Debye model was fit to the measured frequency-dependent complex permittivity. The Debye model parameters obtained from the dielectric properties fit were used in preliminary simulations of the antenna, and then modified slightly within the range of experimental uncertainty of the probe to obtain the best fit between the antenna simulation and measurement data discussed further below. The resulting Debye parameters are as follows: $\varepsilon_\infty = 2.24$, $\varepsilon_s = 2.97$, $\sigma_s = 0$, and $\tau = 5$ ps.

Fig. 1 (solid lines in the top view) shows the topology of a slot-loaded patch antenna comprising two slots (length L_s and width W_s) parallel to and near the radiating edges of the patch and a third slot (length L_c and width W_s) located at the center of the patch. A simpler version of this antenna, consisting of a patch with only two slots near the edges, was studied in [18] and shown to have a dual-band response. In this simpler structure, the lower frequency of operation of the antenna is determined by the resonant frequency, f_{100}, of the dominant mode, TM_{100}, of a rectangular patch antenna while the upper operating frequency is determined by the resonant frequency, f_{300}, of a perturbed higher-order longitudinal mode, TM_{300}. Adding these two slots to the radiating edges of a patch antenna does not

significantly affect the dominant TM_{100} mode because they are located close the current minima; hence, f_{100} is only slightly reduced [18].

The addition of these two slots has a more significant effect on the higher-order mode, TM_{300}, since they are located in regions where the current for that mode is significant. Consequently, the presence of these additional slots reduces f_{300}. Another advantage of adding these slots is that the radiation patterns of the TM_{300} mode can be made similar to that of the TM_{100} mode by judicious choice of the dimensions and location of the slots. However, using the structure presented in [18], the ratio between the two frequencies of operation (f_{300}/f_{100}) can only be changed over a limited range of 1.6–2.0.

The addition of the third slot located at the center of the patch, where both modes have current maxima, as shown in Fig. 2, overcomes this limitation and also further reduces the operating frequencies of the two bands. This slot modifies the current distribution of both the first and third modes and increases their electrical lengths, but does not have any effect on the second mode, TM_{200}, since the slot is located at the current minimum of this mode. Investigations of the effect of the center slot length reveal that as L_c increases, f_{100} and f_{300} are decreased without any significant change on f_{200}, the frequency of the TM_{200} mode. Further increase in the length of the center slot reduces f_{300} until it merges with f_{200}. This is not desired, since the radiation pattern of the TM_{200} mode has a null in the broadside direction that results in minimum power transmission into the breast (compared to that of TM_{100} and TM_{300} modes), even though the input impedance of the antenna is well matched at this mode.

We achieve further miniaturization by adding meandering slots at the non-radiating edges of the patch [19]. Fig. 1(b) shows the location of the meandered slots (dashed lines in the top view) on the miniaturized patch antenna. These slots cause the current paths of all longitudinal modes to be increased, thereby permitting a greater reduction in the length of the patch. Even though the location of the meandering slots do not affect the radiation pattern of the TM_{100} mode, they have a significant effect on the current distribution and the consequent radiation pattern of the third mode, TM_{300}. So, in order to increase the current path without disturbing the current distribution of the third mode, the meandering slots are added around the current minima shown in Fig. 2(b). As the length of these four meandering slots increases, the two operating frequencies of the miniaturized patch antenna are reduced. The combined use of this miniaturization technique and the introduction of the center slot antenna allows this design to achieve dual-band operation with frequency ratios (f_{300}/f_{100}) that can be as small as 1.0 or as large as 2.0. This is in sharp contrast to the design presented in [18] for which a much smaller range of operation is obtained.

A summary of the design guidelines for the proposed antenna is as follows. The resonant frequencies of the three modes are affected by three factors: 1) the length, L_s, of the slot added near the radiating edge, which mainly affects f_{300} and f_{200}, 2) the length, L_c, of the slot added at the center of the patch, which affects f_{100} and f_{300} only, and 3) the length, L_m, of the meandering slots added to the non-radiating edges, which affects all three frequencies. By judicious choice of the length of each of these slots, the frequencies of these three modes as well as the spacing between them can be controlled.

Using CST Microwave Studio, we optimized the dimensions of the miniaturized patch antenna immersed in oil to achieve f_{100} and f_{300} within the 0.5–3.0 GHz frequency range of interest. The resulting physical dimensions are reported in the caption of Fig. 1. Fig. 3 shows the calculated reflection coefficient of the miniaturized patch antenna. The antenna exhibits a multi-band response with TM_{100}, TM_{200}, and TM_{300} resonances at 1.37 GHz, 1.95 GHz, and 2.90 GHz, respectively. Since the radiation pattern of the second mode, TM_{200}, has a

null in the broadside direction, we focus our attention on the first and third modes only. The frequencies of these two modes of interest represent a reduction of 37% and 23%, respectively, relative to the slot-loaded patch antenna reported in [18]. In contrast to [19], our miniaturized design maintains symmetry in the current distribution of both operating modes. This results in symmetric and similar radiation patterns as well as reduced cross polarizations.

III. Measurement and Experimental Verification

We fabricated two prototypes of the dual-band miniaturized patch antenna described in the previous section and measured the reflection and transmission coefficients. Each antenna is patterned on 32-mil-thick RO4003 substrate (Rogers Corp.), and is probe-fed using the center conductor of an SMA connector. We immersed the fabricated antenna(s) in a 32 cm × 15 cm × 11 cm tank filled with safflower oil. The magnitude of the measured S_{11} frequency response of the antenna is shown in Fig. 3. Excellent agreement is observed between the simulated and measured reflection coefficients. The fabricated antenna shows multiple bands at 1.34 GHz, 1.93 GHz, and 2.87 GHz. The slight discrepancy (2% at most) with respect to the simulation results is primarily attributed to the inherent uncertainty in the electrical properties of the oil. Fig. 4 shows the measured transmission coefficient for a system of two miniaturized patch antennas separated by a distance of 10 cm in the oil. As expected, the system has transmission peaks at f_{100} and f300. The transmission peak at f_{200} is very low (–60 dB), confirming that the radiation pattern has a broadside null at this frequency. This second resonance is not useful for the intended application where a low-power microwave signal is transmitted. Here we also observe excellent agreement between simulation and experiment.

We also characterized the radiation patterns of the miniaturized patch antenna immersed in oil. The measurements were taken at a distance of 15 cm from the patch. Fig. 5 shows the co-polarized and cross-polarized radiation patterns in the E- and H-planes at 1.34 GHz and 2.87 GHz. The measured cross-pol level is a minimum of 20 dB lower than co-pol at broadside for both frequencies. We observe better agreement between measurement and simulation in the co-pol radiation patterns than cross-pol. We attribute the greater cross-pol discrepancy to the fact that the very low cross-pol levels are more susceptible to measurement imperfections. As shown in Fig. 5, the antenna exhibits symmetric and similar radiation patterns at the two operating frequencies.

IV. Conclusions

A design of dual-band, miniaturized patch antennas for microwave breast imaging was presented and experimentally verified. The dual-band response is obtained by exploiting the dominant mode, TM_{100}, and one of the higher-order modes of the patch antenna, TM_{300}. Miniaturization is achieved by loading the patch antenna with a series of slots located not only near the radiating edges, as in the case of the dual-band slot-loaded patch [18], but also in the center and along the non-radiating edges of the patch. Appropriate loading locations are chosen to ensure that only the desired resonant modes of the structure are affected and the structure's symmetry is maintained. This ensures that similar and symmetric radiation patterns at both bands of operation are obtained. Using this technique, the resonant frequencies of the TM_{100} and TM_{300} modes of the patch are respectively reduced by 37% and 23%, compared to a conventional dual-band, slot-loaded patch antenna. Two prototypes of this antenna were fabricated and verified experimentally in a biocompatible immersion medium. The measured results of these fabricated prototypes indicate that this structure is a suitable candidate as an array element for multi-frequency microwave breast imaging where high signal-to-noise ratios are desired.

Acknowledgments

This work was supported by the National Institutes of Health under R01 CA112398, the National Science Foundation under a Graduate Fellowship, and Tera-X, LLC (prime contractor: Army Research Office).

References

1. Joy, JE.; Penhoet, EE.; Petitti, DB., editors. Institute of Medicine. Saving Women's Lives: Strategies for Improving Breast Cancer Detection and Diagnosis. Washington, DC: National Academies Press; 2005.
2. Harvey JA, Bovbjerg VE. Quantitative assessment of mammographic breast density: Relationship with breast cancer risk. Radiology. Jan.2004 230:29–41. [PubMed: 14617762]
3. Bulyshev AE, Semenov SY, Souvorov AE, Svenson RH, Nazarov AG, Sizov YE, Tatsis GP. Computational modeling of three-dimensional microwave tomography of breast cancer. IEEE Trans Biomed Eng. Sep; 2001 48(9):1053–1056. [PubMed: 11534841]
4. Zaeytijd JD, Franchois A, Eyraud C, Geffrin JM. Full-wave three-dimensional microwave imaging with a regularized Gauss-Newton method - theory and experiment. IEEE Trans Antennas Propag. Nov; 2007 55(11):3279–3292.
5. Meaney PM, Fanning MW, Raynolds T, Fox CJ, Fang QQ, Kogel CA, Poplack SP, Paulsen KD. Initial clinical experience with microwave breast imaging in women with normal mammography. Academic Radiology. Feb; 2007 14(2):207–218. [PubMed: 17236994]
6. Yu C, Yuan M, Stang J, Bresslour E, George RT, Ybarra GA, Joines WT, Liu QH. Active microwave imaging II: 3-D system prototype and image reconstruction from experimental data. IEEE Trans Microwave Theory Techn. 2008; 56(4):991–1000.
7. Gilmore C, Abubakar A, Hu W, Habashy TM, van den Berg PM. Microwave biomedical data inversion using the finite-difference contrast source inversion method. IEEE Trans Antennas Propagat. 2009; 57(5):1528–1538.
8. Winters DW, Shea JD, Kosmas P, Van Veen BD, Hagness SC. Three-dimensional microwave breast imaging: Dispersive dielectric properties estimation using patient-specific basis functions. IEEE Trans Med Imaging. July; 2009 28(7):969–981. [PubMed: 19211350]
9. Rubaek T, Kim OS, Meincke P. Computational validation of a 3-D microwave imaging system for breast cancer screening. IEEE Trans Antennas Propagat. July; 2009 57(7):2105–2115.
10. Shea JD, Kosmas P, Hagness SC, Van Veen BD. Contrast-enhanced microwave imaging of breast tumors. Inverse Problems. submitted (under review).
11. Fang Q, Meaney PM, Paulsen KD. Singular value analysis of the Jacobian matrix in microwave image reconstruction. IEEE Trans Antennas Propag. Aug; 2006 54(8):2371–2380.
12. Chew, W. Waves and Fields in Inhomogeneous Media. Piscataway, NJ: IEEE Press; 1995.
13. Fang Q, Meaney PM, Paulsen KD. Microwave image reconstruction of tissue property dispersion characteristics utilizing multiple- frequency information. IEEE Trans Microw Theory Tech. Aug; 2004 52(8):1866–1875.
14. Brandstatter B, Hollaus K, Hutten H, Mayer M, Merwa R, Scharfetter H. Direct estimation of Cole parameters in multifrequency EIT using a regularized Gauss-Newton method. Physiological Measurement. May; 2003 24(2):437–448. [PubMed: 12812428]
15. Meaney PM, Paulsen KD, Hartov A, Crane RK. An active microwave imaging system for reconstruction of 2-D electrical property distributions. IEEE Trans Biomed Eng. 1995; 42:1017–1027. [PubMed: 8582719]
16. Li D, Meaney P, Raynolds T, Pendergrass SA, Fanning MW, Paulsen KD. Parallel-detection microwave spectroscopy system for breast imaging. Rev Sci Inst. 2004; 75(7):2305–2313.
17. Behdad N, Shi D, Hong W, Sarabandi K, Flynn MP. A 0.3 mm^2 miniaturized X-band on-chip slot antenna in 0.13 μm CMOS. IEEE RFIC Symposium. June.2007 1:441–444.
18. Maci S, Biffi Gentili G, Piazzesi P, Salvador C. Dual-band slot-loaded patch antenna. IEE Proc Microwave, Antennas and Propagation. June; 1995 142(3):225–232.
19. Dey S, Mittra R. Compact microstrip patch antenna. Microwave Opt Techn Lett. Dec; 1998 13(1): 12–14.

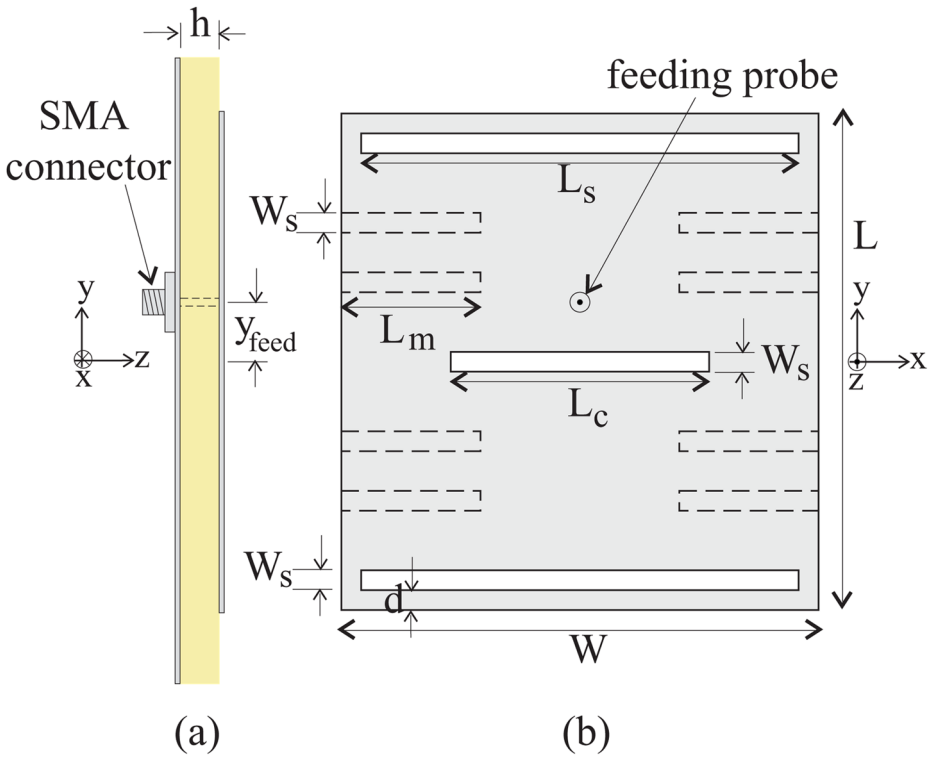

Fig. 1.

(a) Side view, and (b) top view of a dual-band slot-loaded patch antenna (solid lines) and our proposed miniaturized patch antenna (solid and dotted lines). W=28 mm, L=29 mm, W_s=1 mm, L_s=24 mm, L_c=12 mm, d=2 mm, L_m=10 mm, h=0.81 mm. y_{feed} represents the feed location, where y_{feed}=9.5 mm for the slot-loaded patch antenna and y_{feed}=4.5 mm for the proposed miniaturized patch antenna.

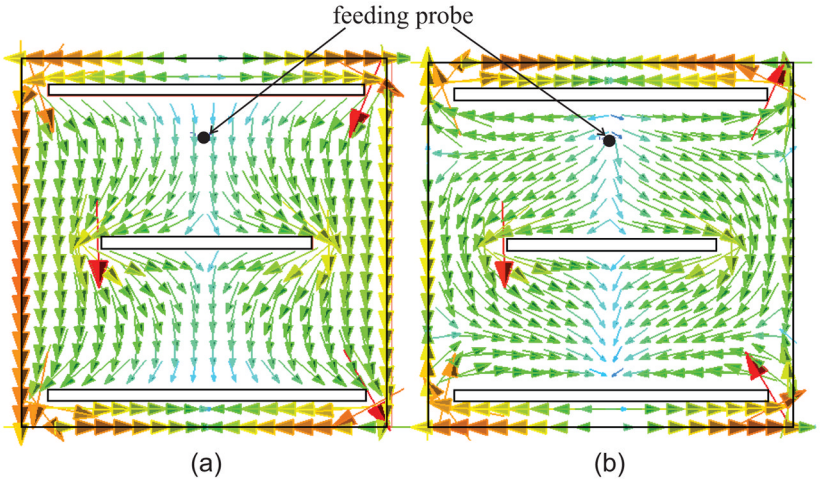

Fig. 2.
Current distribution of the dual-band slot-loaded patch antenna. (a) TM_{100} mode; (b) TM_{300} mode.

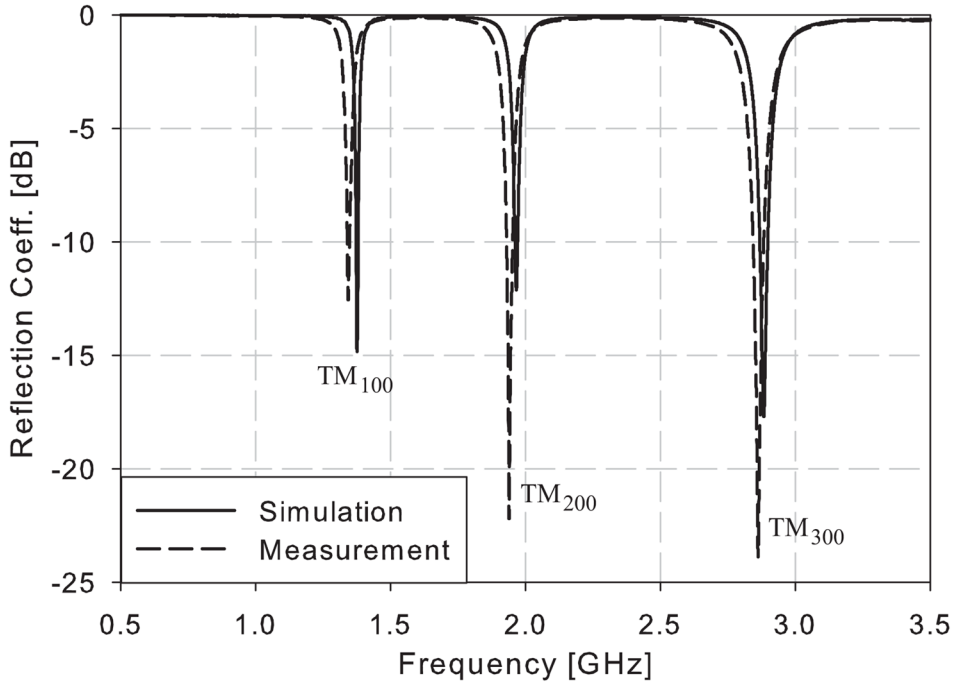

Fig. 3.
Simulated and measured reflection coefficients of the miniaturized patch antenna of Fig. 1 immersed in safflower oil.

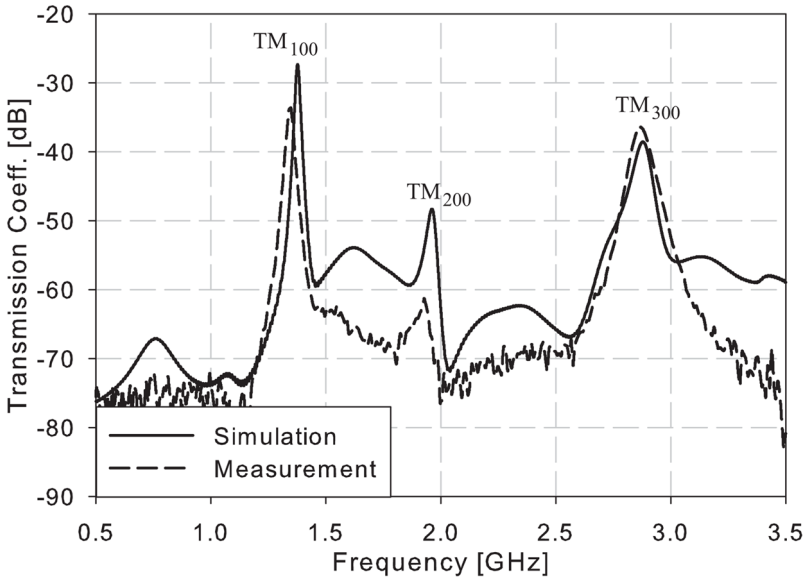

Fig. 4.

Simulated and measured transmission coefficients of a two-antenna system. The two miniaturized patch antennas are immersed in safflower oil and separated by 10 cm.

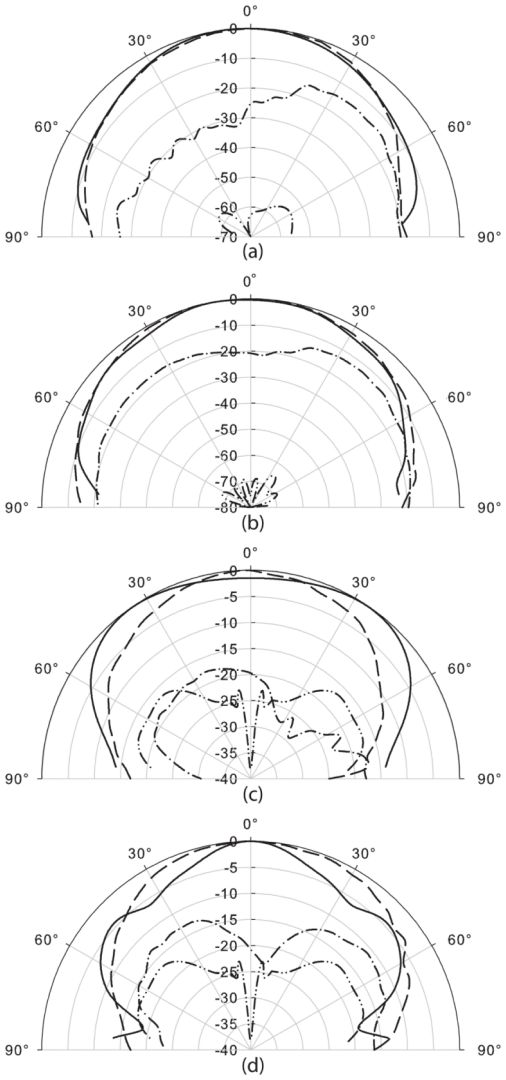

Fig. 5.

Measured and simulated radiation patterns of the dual-band miniaturized patch antenna in oil. The patterns are obtained at a distance of 15 cm from the patch. (a) E-plane at 1.34 GHz (b) E-plane at 2.87 GHz (c) H-plane at 1.34 GHz (d) H-plane at 2.87 GHz. Dash-dash: measured co-pol. Solid: simulated co-pol. Dash-dot-dash: measured cross-pol. Dash-dot-dot-dash: simulated cross-pol.